Journal of Materials Chemistry A

Accepted Manuscript

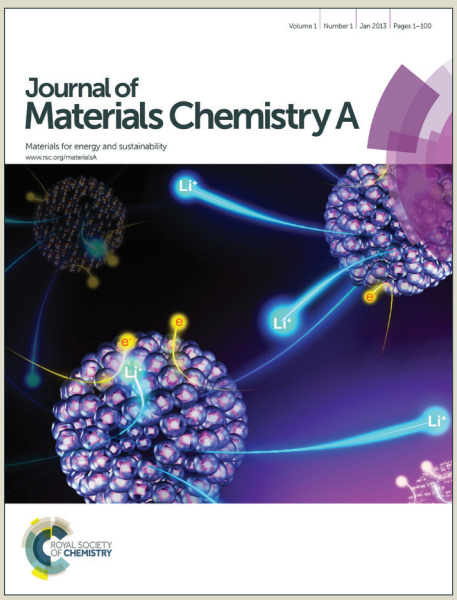

ROYAL SOCIETY OF CHEMISTRY

www.rsc.org/materialsA

Journal Name

RSCPublishing

ARTICLE

Environment-benign synthesis of branched Bi_2O_3-Bi_2S_3 photocatalysts by an etching and re-growth method

Cite this: DOI: 10.1039/x0xx00000x

Received 00th January 2012,
Accepted 00th January 2012

DOI: 10.1039/x0xx00000x

www.rsc.org/

Lang Chen, Jie He, Qing Yuan, Ying Liu, Chak-Tong Au and Shuang-Feng Yin*

To synthesize heterostructured nanomaterials of controllable morphologies by an environment-benign method is an area of frontier research. In the present work, Bi_2O_3 microtubes and branched Bi_2O_3-Bi_2S_3 composites were synthesized by a simple hydrothermal method without the need of using toxic substances as surfactant (template) or solvent. Single-crystalline Bi_2S_3 nanorods and nanosheets are controllably grown on the surface of Bi_2O_3 microtubes. We propose an "etching and re-growth" mechanism for the generation of the Bi_2O_3-Bi_2S_3 composites. Owing to the presence of Bi_2S_3 and the branched structure, there is great improvement of visible-light absorption ability, and due to the formation of Bi_2O_3-Bi_2S_3 heterojunctions, there is facile separation of photogenerated charge carriers. It is observed that the as-prepared composites show enhanced photocurrent response and improved photocatalytic activity under visible-light illumination.

Introduction

The construction of heterostructrued semiconductors by an environment-benign method is a challenge in material and chemical engineering. With the formation of an appropriate hetero-structure, there could be staggered alignment of band gaps, and hence efficient separation of photogenerated charge carriers.[1] Also, due to multiple refraction of incident light, hybrids of heterostructured materials with hollow and branched structures show improved light absorption ability.[2] Furthermore, when a semiconductor of narrow band gap is used, there is widening of light absorption range and better utilization of visible light.[3] It is known that a combination of these effects can result in enhancement of photocatalytic activity when the heterostructrued semiconductors are used as high-efficiency photocatalysts.

As an important member of V-VI semiconductor materials, bismuth sulfide (Bi_2S_3) is well studied for its potential application in X-ray computed tomography imaging,[4] Schottky diodes,[5] lithium ion batteries,[6] gas sensors,[7] thermoelectricity,[8] and electrochemical hydrogen storage.[9] Having a direct narrow band-gap (1.3-1.7 eV), Bi_2S_3 absorbs visible light ($\lambda \lesssim 800$ nm) and can be used as visible-light photocatalysts. Since the first report by Wu et al[10] on the use of Bi_2S_3 nanodots and nanorods as photocatalysts for the degradation of dyes under UV light, there are much progresses.[11] However, due to the facile recombination of photogenerated electrons and holes (a result of narrow band gap between the conduction band and valance band of Bi_2S_3), the photocatalytic performance of single-crystalline Bi_2S_3 under UV and visible light is not satisfactory. In spite of this, Bi_2S_3 is used as a visible-light sensitizer for photocatalysts, e.g. $BiVO_4$/Bi_2S_3,[3a] Bi_2S_3/Bi_2WO_6,[3c] Bi_2S_3-TiO_2,[12] Bi_2S_3-$Bi_2O_2CO_3$[13] and Bi_2S_3-Bi_2O_3.[14] Looking into the methods developed so far for the generation of this kind of composites, one can see shortcomings such as the use of harmful solvents and additives as well as the need of complex processes in synthesis. It is hence of interest to look for methods that are simple and environmentally benign.

It is known that Bi_2O_3 shows low absorption of visible light (2.58-2.85 eV),[15] and Bi_2S_3 has serious problem with the recombination of charge carriers.[11] Nonetheless, considering the incommensurable solubility (K_{sp}: 4×10^{-31} and 1×10^{-97}, respectively) and structure similarity of Bi_2O_3 and Bi_2S_3, it is envisaged that it is possible to synthesize Bi_2O_3-Bi_2S_3 composites that are free of those shortcomings. In the present work, we developed a hydrothermal process for the controlled growth of Bi_2S_3 on the surface of Bi_2O_3 by an "etching and re-growth" mechanism. It is the first report on the synthesis of Bi_2O_3 microtubes and branched Bi_2O_3-Bi_2S_3 composites without the employment of toxic solvent or surfactant.

Experimental

The Bi_2O_3-Bi_2S_3 (BO-BS) composites were prepared by a two-step hydrothermal method. The first step was the preparation of Bi_2O_3 (BO) microtubes. The second step was the growth of Bi_2S_3 (BS) on the obtained BO substrates. The as-prepared samples were characterized using XRD, FT-IR, XPS, SEM, TEM (HRTEM), UV-vis DRS, PL techniques. Degradation of Rhodamine B (RhB) was used as probe reaction to evaluate the photocatalytic activity of the as-synthesized samples. Photodegradation processes were conducted using a home-made Pyrex glass vessel with temperature maintained at room temperature by means of an external water flow as described elsewhere.[16] Further details are available in the Electronic Supplementary Information (ESI).

Results and discussion

Composition: Figure 1a shows the XRD patterns of the prepared BO, BO-BS and BS samples. The patterns of BO and BS can be indexed to monoclinic Bi_2O_3 and orthorhombic Bi_2S_3 (JCPDS card No. 65-2366 and 65-2431), respectively. No signals other than that of Bi_2O_3 and Bi_2S_3 phases can be detected, indicating that the samples are phase-pure. For the composite samples, no apparent peaks ascribable to Bi_2S_3 is detected. **Figure 1b** shows the FT-IR spectra of the BO-BS composites. The spectrum of pure BO is in agreement with that reported in the literature [17] and peaks at 514 and 549 cm^{-1} are characteristic of υ(Bi-O). Peaks at 3491 and 1653 cm^{-1} that appear in the spectra of BS and BO-BS are corresponding to υ(O-H) stretching and ä(O–H) bending vibrations, respectively, plausibly due to the adsorption of a small amount of water on the surface of the samples.[18] We detected no 3491 and 1653 cm^{-1} peaks in the BO spectrum, and the result suggests that water adsorption on BO is relatively unfavorable. In addition, the 638 and 1136 cm^{-1} peaks of pure BS assignable to Bi-S bond vibrations[18] are detected over the composite sample, indicating successfully generation of the BO-BS composite. **Figure 1c** and **d** are the XPS spectra of the synthesized samples. From the survey scans (**Figure 1c**), one can see Bi, O and C on the BO and BO-BS samples, and there are weak peaks at around 225 eV detected over the composite samples but not over BO. As shown in the high-resolution S2s spectra (**Figure 1d**), the peak at a binding energy of 226.1 eV is characteristic of S^{2-}. In other words, the FT-IR and XPS results confirm the presence of Bi_2S_3 on Bi_2O_3. The Bi_2S_3 to Bi_2O_3 molar ratios of BO-BS as measured by X-ray Fluorescence analysis are 0.18:1 and 0.20:1 for BO-BS (TU) and BO-BS (SS) respectively.

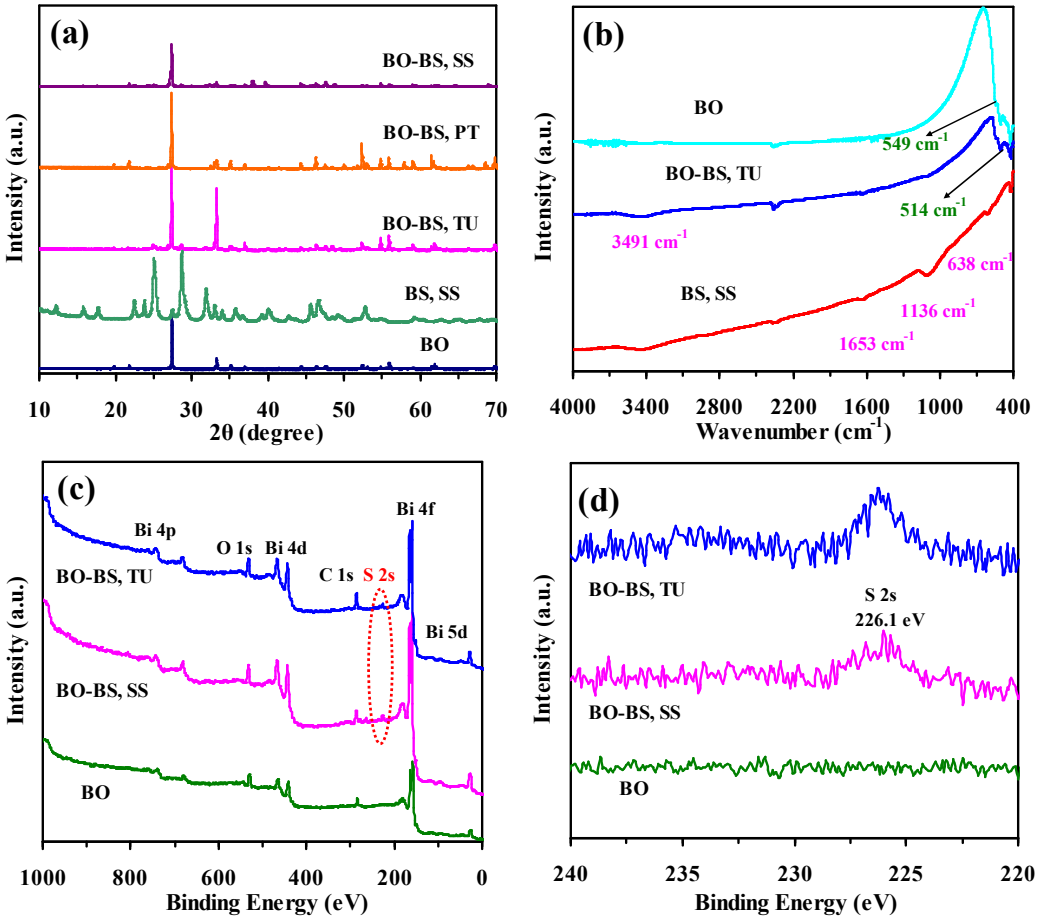

Figure 1. (a) XRD, (b) FT-IR, (c) XPS survey scan and (d) XPS S 2s spectra of the prepared BO, BS and BO-BS composites synthesized using different sulfur sources (SS, TU and PT stand for sodium sulfide, thiourea and potassium thiocyanate, respectively).

Morphology: Displayed in **Figure 2** are the images of composite samples prepared using different sulfur sources. The BO-BS samples exhibit branched structures with hollow interiors, having the basic structure of BO microtubes remaining intact. The high-resolution SEM images of the composite prepared using SS as sulfur sources (**Figure 2b**) demonstrates that there are micro- and nano-needles with diameter range of 1-4 µm radially grown on the Bi_2O_3 matrix. For comparison, the SEM images of BO microtubes are shown in **Figure S1**, ESI. The EDS analysis of the needles (**inset** of **Figure 2b**) suggests that the needles are composed of Bi and S elements. The results confirm the formation of Bi_2S_3 on Bi_2O_3. The composite was further characterized by elemental mapping and results are shown in **Figure S2** (ESI). The clear distribution of Bi, S and O suggests the growth of Bi_2S_3 on the surface of Bi_2O_3. The TEM result (**Figure 2c** (inset)) provides clear indication of the presence of Bi_2O_3 matrix and Bi_2S_3 needles, in consistent with the SEM findings. The HRTEM image of a single needle (**Figure 2d**) shows lattice fringes of 0.375 nm corresponding to the (011) crystal plane of Bi_2S_3.

The inset of **Figure 2d** shows the relevant FastFourier Transform (FFT) image, and the bright spots indicate single-crystallinity of the Bi_2S_3 needles. When PT and TU are used as sulfur sources (**Figure 2f** and **h**), Bi_2S_3 appears as irregular and uniformed nanosheets, respectively, on the surface of Bi_2O_3. The sheets intercross with one another and there are regular interspaces on the surface. It is believed that the existence of Bi_2S_3 in such a way favors light refraction, and the outcome is enhancement of light-absorption ability.

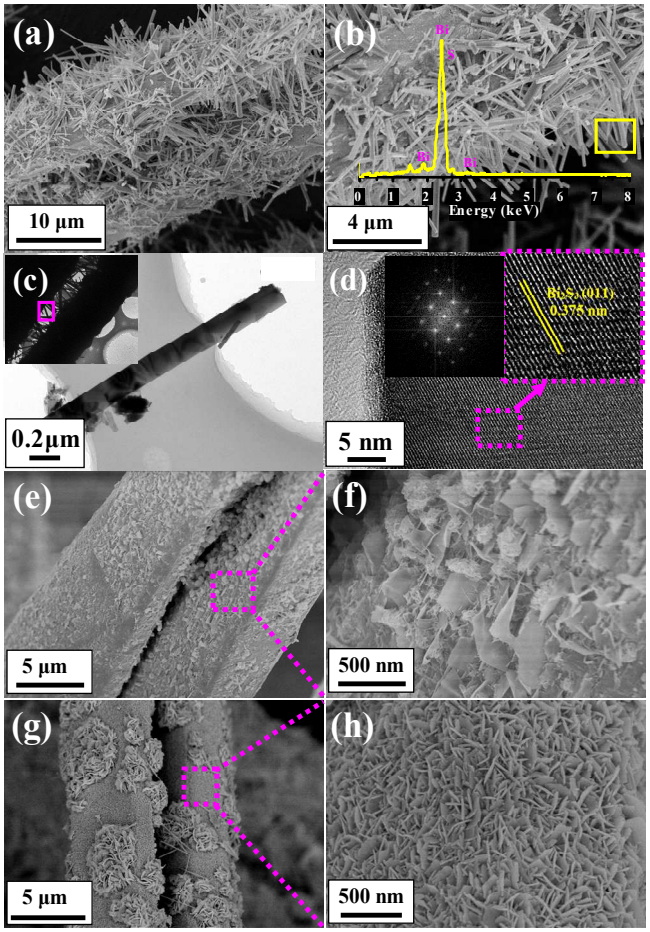

Figure 2. (a) & (b) SEM and (c) & (d) TEM images of BO-BS composites prepared using sodium sulphide as sulfur source. Also SEM images of BO-BS prepared using (e) & (f) potassium thiocyanate and (g) & (h) thiourea as sulfur source.

Growth Mechanism: It is important to make clear the growth mechanism of the nanomaterials so as to controllably synthesize other nanomaterials of novel structures. **Figure 3** shows the images of BO and BO-BS composites collected at different crystallization periods. The surface of BO is initially smooth (**Figure 3a**) but starts to get roughened after hydrothermal treatment at 160 ºC for 1 h. There is the appearance of small particles of irregular size on the surface (**Figure 3b**). At a hydrothermal treatment time of 3 h, there is a large amount of micro- and nano-needles which are 1-2 μm in length and 100-200 nm in width on the surface (**Figure 3c, d**). At 6 h, the BS needles become ca. 5 μm in length and ca. 500 nm in width, and the hollow interior of BO remains intact (**Figure 3e, f, g**). It is worth pointing out that there is no extra addition of bismuth source in the growth process. In other words, BO acts as a substrate as well as a bismuth source for the growth of BS needles.

It is known that in aqueous solution the solubility of BS ($K_{sp}=1\times10^{-97}$) is much lower than that of BO ($K_{sp}=4\times10^{-31}$). With the feasibility of BS generation on BO in a sulfur-containing solution ensured, we propose an "etching and re-growth" mechanism for the formation of the branched BO-BS composites. As displayed in **Figure 3h**, there is the equilibrium of BO and Bi^{3+} on the BO surface. When BO is placed in a solution containing a large amount of S^{2-}, there is transfer of S^{2-} towards the BO surface (**Figure 3i**). Due to solubility disparity, there is immediate formation of BS nuclei on BO, and the balance between BO and Bi^{3+} is shifted towards Bi^{3+} formation. In other words, through the formation of BS, there is promotion of BO dissolution. The generation of BS is a result of Bi^{3+} reacting with S^{2-} (**Figure 3j**). With the lengthening of synthesis time, the BS needles become larger as revealed in the SEM results. When different sulfur sources are used, the produced BS grows along different plane directions, resulting in BS of different morphologies. In this "etching and re-growth" process, the BO matrix is etched and the BS grows on it, the driving force is originated from the difference in solubility.

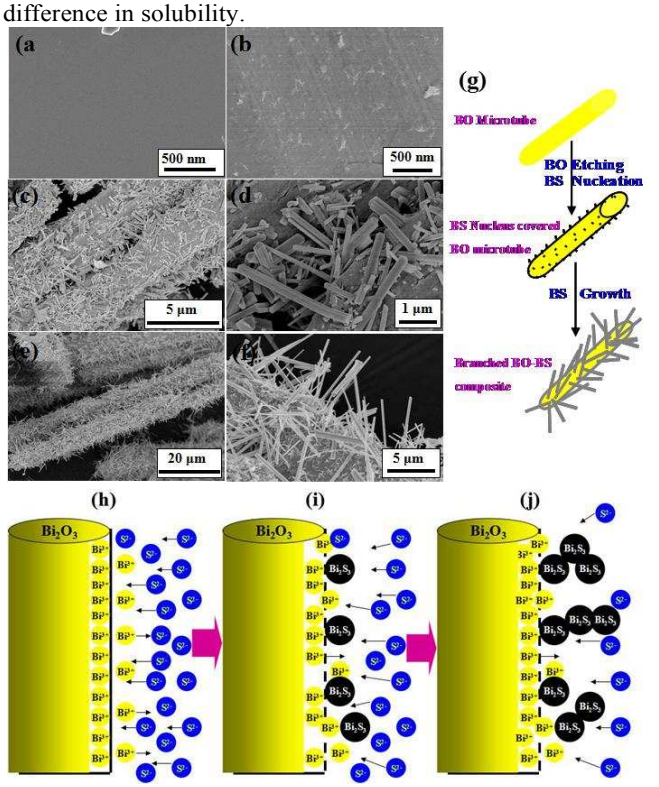

Figure 3. SEM images of (a) BO and also BO-BS prepared using sodium sulphide as sulfur source after crystallization for (b) 1 h, (c) & (d) 3 h, and (e) & (f) 6 h. Also shown are (g) sketch map, and (h), (i), & (j) etching and re-growth mechanism for the branched BO-BS composites.

To confirm this mechanism, we studied the effect of sulfur concentration on the BO-BS composites. In the XRD patterns of the BO-BS composites, besides the BO peaks, there are peaks ascribable to BS (**Figure S3**, **ESI**). Shown in **Figure S4** (ESI) are the SEM images of BO and BO-BS samples (prepared using SS as sulfur source). The surface of BO is smooth and only Bi and O elements are detected in EDS analysis (**Figure S4b** and **c**, ESI). At relatively low SS concentration, the obtained composite keeps the original hollow structure of BO, but there are swelling of surface as if there is the presence of a rough film (**Figure S4d-f**, ESI). At higher SS concentration, there is a large amount of nanorods whose

length increases with the increase of SS concentration (**Figure S4g-o**, ESI). Within the adopted crystallization time, a higher SS concentration means higher rate of BS formation and thus longer BS rods. The results further confirm the proposed etching and re-growth mechanism

Optical Properties: Light absorption behavior is an important factor affecting the activity of a photocatalyst. **Figure 4a** displays the UV-vis absorption property of the prepared samples. It is clear that pure BO shows strong absorption at a wavelength lower than

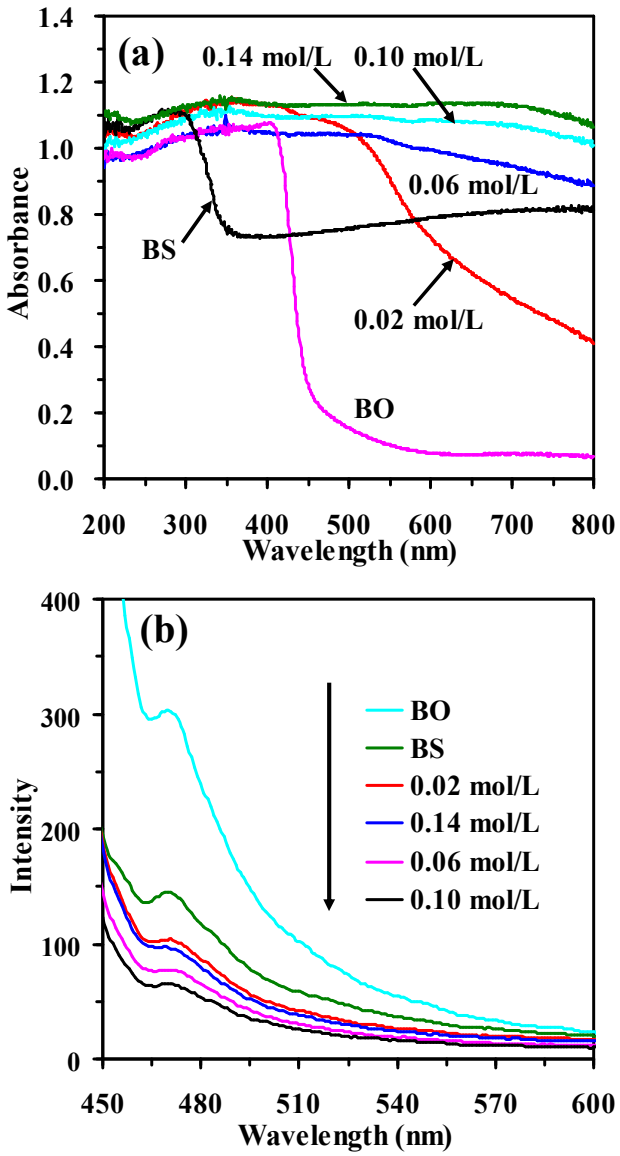

Figure 4. (a) UV-vis absorption property and (b) room-temperature PL spectra of BO, BS and BO-BS composites prepared using different concentrations of sodium sulphide.

450 nm, and BS shows strong absorption in the 200-800 nm region, in agreement with the reported results.[14,19] When BO is treated in SS solution of low concentration (0.02 mol/L), there is red shift of light absorption, and the absorption strength is lower than that of pure BS. With the increase of SS concentration, the BO-BS composites not only show light absorption region as wide as BS but also exhibit absorption intensity stronger than that of BO or BS, especially so in the visible region. The wide absorption is ascribed to the presence of BS which is a typical semiconductor of narrow band gap, while the strong absorption is due to the novel structures (hollow and branched) that enable light scattering.[20] Being strong in light absorption ability, the composites produce more photogenerated charge carriers than the individual components.

It is envisaged that the separation of charge carriers plays a crucial role in achieving high efficiency over visible-light driven photocatalysts of this kind. Photoluminescence (PL) is commonly used to study the recombination of charge carriers, the lower PL intensity the higher the efficiency in charge separation. [21] Using this technique, we investigated the separation properties of charge carriers. Shown in **Figure 4b** are the room-temperature PL spectra of the prepared samples (excited at 425 nm). It is clear that the composites show lower PL intensity than BO and BS, indicating efficient separation of photogenerated electrons and holes. Among the BO-BS composites, the one prepared at SS concentration of 0.10 mol/L shows the lowest PL intensity.

Photocatalytic Properties: Photocatalytic degradation of Rhodamine B (RhB) was taken as a probe reaction to evaluate the visible-light driven photocatalytic activity of the samples. One can see from **Figure 5a** that photolysis of RhB under visible light is not significant. In the photocatalytic reactions, the BO-BS composites show higher activity than BO and BS, and the BO-BS composite prepared with SS concentration of 0.10 mol/L shows the highest activity, in consistence with the PL results. Photocatalytic activities of the composites prepared using different sulfur sources are displayed in **Figure 5b**. It is clear that all the composites show much higher activity than the individual components. It is worth pointing out that the highest activity is achieved over the composite prepared using TU as sulfur source. This can be attributed to the fact that the uniform BS nanosheets on BO are more efficient than the nanrods in terms of light harvesting.

The stability and reusability or the as-prepared composite was investigated in four cycles. The catalyst was collected by simple filtration. The BO-BS photocatalyst obtained using thiourea as sulfur source shows good stability. Even it shows a little loss of photocatalytic activity (from 99% to 85%) in the fourth cycle, the residual dye can be removed by prolonging the irradiation time (**Figure S5**, ESI).

Photocurrent Response: To find out whether efficient separation of charge carriers is an important factor for the higher activity, we measured the photocurrent[22] of the samples (**Figure 6a**). Under visible-light irradiation, all samples show reversible photoresponses that are reproducible, indicating that the samples (electrodes) are stable. Even though BS shows wider absorption than BO, its photocurrent intensity is similar to that of BO (0.001 $\mu A/cm^2$). This is ascribed to the narrow gap between the conduction and valence bands that enables easy recombination of photogenerated electrons and holes. The photocurrent densities of the composites prepared using SS, PT and TU as sulfur sources are 0.1, 0.2 and 0.5 $\mu A/cm^2$, respectively, which are 100-500 times that of BO and BS. The high photocurrent densities can be related to the strong absorption of visible light and the efficient separation of charge carriers. According to the above discussion, a possible mechanism for enhanced photocatalytic activity of the BO-BS photocatalysts is proposed and shown in **Figure 6**. One can see from **Figure 6b** that due to light reflection, the amount of harvested light on bare BO is limited. With BS rods anchored on the BO surface, much more incident light can be absorbed because the incident path is greatly lengthened due to multiplex refraction. The results of UV-vis absorption provide strong evidence for this mechanism. Namely, the amount of photoinduced charge carriers detected over the composite catalyst is much more than that over pure BO and BS. Due to band energy difference between BO and BS (**Figure 6c**, both the CB and VB of BO are more positive than

BS), there is fast transfer of photogenerated electrons from BS to BO and holes from BO to BS at the BO-BS heterojunctions, resulting in efficient separation of charge carriers.

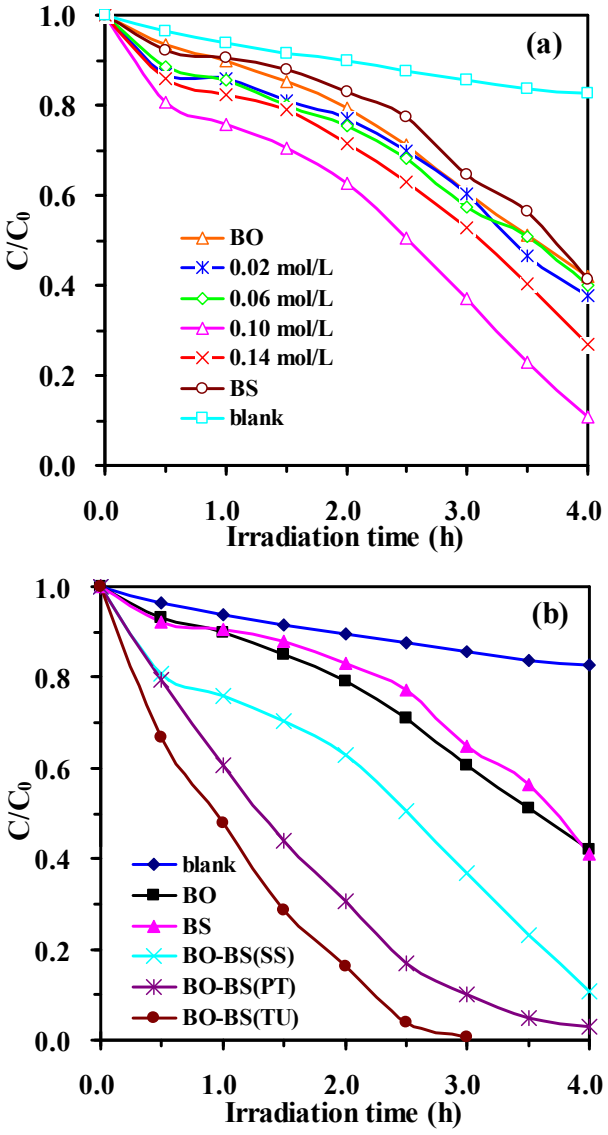

Figure 5. Photocatalytic degradation of RhB recorded over (a) BO, BS and BO-BS composites prepared using different concentrations of sodium sulphide, (b) BO-BS composites prepared using different sulfur sources (SS, TU and PT stand for sodium sulfide, thiourea and potassium thiocyanate, respectively.).

Conclusions

In summary, a green hydrothermal method has been developed for the synthesis of Bi_2O_3 microtubes and branched Bi_2O_3-Bi_2S_3 composites without the use of organic solvent and/or toxic surfactant (or template). By varying the kind and concentration of sulfur source, Bi_2S_3 nanosheets and nanorods of single-crystal nature are controllably synthesized on the surface of Bi_2O_3 microtubes. Based on the characterization results, we propose an etching and re-growth mechanism. Due to the strong visible-light absorption ability of Bi_2S_3, multiplex reflection of incident light (because of the branched structure) and the presence of heterojunctions between Bi_2O_3 and Bi_2S_3, the composites show much higher activity than the individual components towards the degradation of RhB under visible-light irradiation. The present study provides a novel and environment-friendly way for the preparation of heterostructured nanomaterials with novel structures.

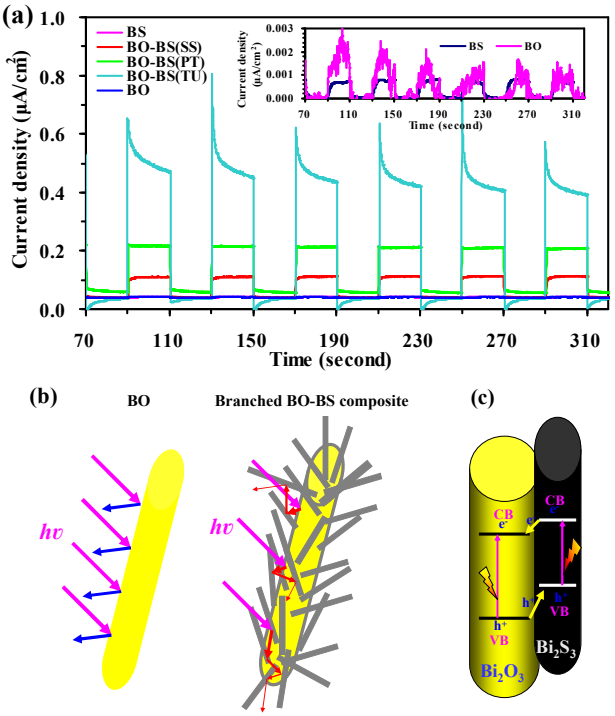

Figure 6. (a) Transient photocurrent responses of the as-prepared samples when illuminated by visible light (500 W Xe lamp, λ≥420 nm), (b) enhancement process for light absorption, and (c) charge carrier separation process for the BO-BS composites. (SS, TU and PT stand for sodium sulfide, thiourea and potassium thiocyanate, respectively.)

Acknowledgements

This project was financially supported by NSFC (Grant Nos. U1162109, 21273067 and J1210040) and the Fundamental Research Funds for the Central Universities. C.T. Au thanks the HNU for an adjunct professorship.

Notes and references

State Key Laboratory of Chemo/Biosensing and Chemometrics, College of Chemistry and Chemical Engineering, Hunan University, Changsha (410082), People's Republic of China.
* Coresponding Author: E-mail: sf_yin@hnu.edu.cn (Shuang-Feng Yin).
Electronic Supplementary Information (ESI) available: [Details for preparation, characterization and evaluation of the photocatalysts, SEM images, XRD patterns]. See DOI: 10.1039/b000000x/

1. a) Y. Qu and X. Duan, *Chem. Soc. Rev.*, 2013, **42**, 2568; b) J. Zhang, Z.P. Zhu, Y.P. Tang, K. Mullen and X.L. Feng, *Adv. Mater.*, 2014, **26**, 734; c) G. Manna, R. Bose and N. Pradhan, *Angew. Chem. Int. Ed.*, 2014, **53**, 6743; d) H.R. Yang, S.W. Finefrock, J.D. Albarracin Caballero and Y. Wu, *J. Am. Chem. Soc.*, 2014, **136**, 10242; e) N.J. Huo, Q. Yue, J.H. Yang, S.X. Yang and J.B. Li, *ChemPhysChem*, 2013, **14**, 4069; f) S.X. Yang, H.Y. Yang, H.Y. Ma, S. Guo, F. Cao, J.

Gong and Y.L. Deng, *Chem. Commun.*, 2011, **47**, 2619.

2. a) U.K. Gautam, X.S. Fang, Y. Bando, J.H. Zhan and D. Golberg, *ACS Nano,* 2008, **2**, 1015; b) W.J. Zhou, Z.Y. Yin, Y.P. Du, X. Huang, Z.Y. Zeng, Z.X. Fan, H. Liu, J.Y. Wang, H. Zhang, *Small,* 2013, **9**, 140; c) W. Tan, C. Zhang, T.Y. Zhai, S.L. Li, X. Wang, J.W. Liu, X. Jie, D.Q. Liu, M.Y. Liao, Y. Koide, D. Golberg and Y. Bando, *Adv. Mater*., 2014, **26**, 3088
3. a) X.H. Gao, H.B. Wu, L.X. Zheng, Y.J. Zhong, Y. Hu, and X.W. Lou, *Angew. Chem. Int. Ed*., 2014, **53**, 5917; b) W.X. Guo, C. Xu, X. Wang, S.H. Wang, C.F. Pan, C.J. Lin and Z.L. Wang, *J. Am. Chem. Soc*., 2012**, 134**, 4437; c) Z.J. Zhang, W.Z. Wang, L. Wang, and S.M. Sun, *ACS Appl. Mater. Interfaces* 2012, **4**, 593; d) R. Marschall, *Adv. Funct. Mater*., 2014, **24**, 2421; e) N. Liang, M. Wang, L. Jin, S.S. Huang, W.L. Chen, M. Xu, Q. Q. He, J.T. Zai, N.H. Fang and X.F. Qian, *ACS Appl. Mater. Interfaces*, 2014, **6**, 11698.
4. O. Rabin, J.M. Perez, J. Grimm, G. Wojtkiewicz and R. Weissleder, *Nature Mater.,* 2006, **5**, 118.
5. H.F. Bao, C.M. Li, X.Q. Cui, Y. Gan, Q.L. Song and J. Guo, *Small,* 2008, **4**, 1125.
6. a) J.F. Ni, Y. Zhao, T.T. Liu, H.H. Zheng, L.J. Gao, C.L. Yan and L. Li, *Adv. Energy Mater.,* 2014, DOI: 10.1002/aenm.201400798; b) J.M. Ma, Z.F. Liu, J.B. Lian, X.C. Duan, T. Kim, P. Peng, X.D. Liu, Q. Chen, G. Yao and W.J. Zheng, *CrystEngComm* 2011, **13**, 3072.
7. K. Yao, W.W. Gong, Y.F. Hu, X.L. Liang, Q. Chen and L.M. Peng, *J. Phys. Chem. C,* 2008, **112**, 8721.
8. K. Biswas, L.D. Zhao and M.G. Kanatzidis, *Adv. Energy Mater.,* 2012**, 2**, 634.
9. B. Zhang, X.C. Ye, W.Y. Hou, Y. Zhao and Y. Xie, *J Phys Chem B,* 2006, **110**, 8978.
10. T. Wu, X. Zhou, H. Zhang and X. Zhong, *Nano Res*., 2010, **3**, 379.
11. a) Chen, F.J.; Y.L. Cao and D.Z. Jia, *J. Colloid Interface Sci.,* 2013, **404**, 110; b) Y.F. Luo, H. Chen, X. Li, Z.Q. Gong, X.J. Wang, X.F. Peng, M.D. He and Z.Z. Sheng, *Mater. Lett*., 2013, **105**, 12; c) J. Huang, H. Zhang, X.G. Zhou and X.H. Zhong, *Mater. Chem. Phys*., 2013, **138**, 755; d) G. Manna, R. Bose and N. Pradhan, *Angew. Chem. Int. Ed.,* 2014, **53**, 6743.
12. a) X. Li, H.L. Liu, D.L. Luo, J.T. Li, Y. Huang, H.L. Li, Y.P. Fang, Y.H. Xu and L. Zhu, *Chem. Eng. J*., 2012, **180**, 151; b) H.J. Yu, J. Huang, H. Zhang, Q.F. Zhao and X.H. Zhong, *Nanotechnology,* 2014, **25**, DOI: 10.1088/0957-4484/25/21/215702.
13. N. Liang, JT. Zai, M. Xu, Q. Zhu, X. Wei and X.F. Qian, *J. Mater. Chem. A,* 2014, **2**, 4208.
14. a) X.Q. Lu, F. Pu, Y. Xia, W. Huang and Z.L. Li, *Appl. Surf. Sci.* 2014, **299,** 131; b) F.Y. Lu, R.X. Li, N.J. Huo, J.H. Yang, C. Fan, X.Z. Wang, S.X. Yang and J.B. Li, *RSC Adv*., 2014, **4,** 5666.
15. a) Y.F. Qiu, D.F. Liu, J.H. Yang and S.H. Yang, *Adv. Mater.,* 2006, **18**, 2604; b) J.G. Hou, C. Yang, Z. Wang, W.L. Zhou, S.Q. Jiao and H.M. Zhu, *Appl. Catal. B,* 2013, **142**, 504.
16. L. Chen, R. Huang, Q. Yuan, J. He, J. Jia, M.Y. Yao, S.L. Luo, C.T. Au and S.F. Yin, *Inorg. Chem*., 2013, **52**, 11118.
17. L. Huang, G.S. Li, T.J. Yan, J. Zheng and L.P. Li, *New J. Chem.,* 2011, **35**, 197.
18. J. Cao, B.Y. Xu, H.L. Lin, B.D. Luo and S.F. Chen, *Dalton Trans*., 2012, **41**, 11482.
19. J. Wang, X..Yang, K. Zhao, P. Xu, L. Zong, R. Yu, D. Wang, J. Deng, J. Chen and X. Xing, *J. Mater. Chem. A,* 2013, **1**, 9069.
20. a) Y.L. Min, G.Q. He, Q.J. Xu and Y.C. Chen, *J. Mater. Chem. A,* 2014, **2,** 2578; b) Y.X. Zhao, W.T. Wang, Y.P. Li, Y. Zhang, Z.F. Yan and Z.Y. Huo, *Nanoscale,* 2014, **6**, 195; c) Y. Hou, F. Zuo, A. Dagg and P.Y. Feng, *Angew. Chem. Int. Ed.,* 2013, **52**, 1248.
21. a) L. Chen, S.F. Yin, S.L. Luo, R. Huang, Q. Zhang, T. Hong and C.T. Au, *Ind. Eng. Chem. Res.,* 2012, 51, 6760; b) M. Xiong, L. Chen, R. Huang, Q. Yuan, J. He, S.L. Luo, C.T. Au and S.F. Yin, *Dalton Trans.,* 2014, **43**, 8331; c) Q. Yuan, L. Chen, M. Xiong, J. He, S.L. Luo, C.T. Au and S.F. Yin, *Chem. Eng. J.,* 2014, **256**, 394.
22. a) H. Park and W. Choi, *J. Phys. Chem. B,* 2003, **107**, 3885; b) J.K. Liu, S.H. Wen, Y. Hou, F. Zuo, G.J.O. Bera and P.Y. Feng, *Angew. Chem.,* 2013, **125**, 3323; c) Y. Wang, J.S. Zhang, X.C. Wang, M. Antonietti and H.R. Li, *Angew. Chem. Int. Ed.,* 2010, **49**, 3356; d) S.X. Yang, X.J. Cui, J. Gong and Y.L. Deng, *Chem. Commun.*, 2013, **49**, 4676.

